ARTICLES
PUBLISHED ONLINE: 6 APRIL 2015 | DOI: 10.1038/NMAT4251
nature materials

Flexible n-type thermoelectric materials by organic intercalation of layered transition metal dichalcogenide TiS_2

Chunlei Wan[1,2*], Xiaokun Gu[3], Feng Dang[1], Tomohiro Itoh[1], Yifeng Wang[4], Hitoshi Sasaki[1], Mami Kondo[1], Kenji Koga[5], Kazuhisa Yabuki[5], G. Jeffrey Snyder[6], Ronggui Yang[3] and Kunihito Koumoto[1*]

Organic semiconductors are attracting increasing interest as flexible thermoelectric materials owing to material abundance, easy processing and low thermal conductivity. Although progress in p-type polymers and composites has been reported, their n-type counterpart has fallen behind owing to difficulties in n-type doping of organic semiconductors. Here, we present an approach to synthesize n-type flexible thermoelectric materials through a facile electrochemical intercalation method, fabricating a hybrid superlattice of alternating inorganic TiS_2 monolayers and organic cations. Electrons were externally injected into the inorganic layers and then stabilized by organic cations, providing n-type carriers for current and energy transport. An electrical conductivity of 790 S cm^{-1} and a power factor of 0.45 mW m^{-1} K^{-2} were obtained for a hybrid superlattice of TiS_2/[(hexylammonium)$_x$(H_2O)$_y$(DMSO)$_z$], with an in-plane lattice thermal conductivity of 0.12 ± 0.03 W m^{-1} K^{-1}, which is two orders of magnitude smaller than the thermal conductivities of the single-layer and bulk TiS_2. High power factor and low thermal conductivity contributed to a thermoelectric figure of merit, *ZT*, of 0.28 at 373 K, which might find application in wearable electronics.

Organic semiconductors, such as conjugated polymers, have been successfully applied to thin-film electronics[1–3] and optoelectronic devices[4,5] and are attracting attention as a potential thermoelectric material[6,7]. Owing to their flexibility and easy processing, organic semiconductors and composites can offer new opportunities for flexible power generation, Peltier cooling and sensor networks for wearable technologies, which is not possible with the conventional brittle and usually toxic inorganic thermoelectric materials. Thermoelectric energy conversion efficiency is determined by the thermoelectric figure of merit (ZT), defined as $S^2\sigma T/\kappa$, where S, σ, T and κ represent Seebeck coefficient, electrical conductivity, absolute temperature and thermal conductivity, respectively. Great progress has been made on p-type polymers and composites, especially those based on poly(3,4-ethylenedioxythiophene) polystyrene sulphonate (PEDOT–PSS), with the highest ZT reported to be 0.42 (refs 6,7). However, an n-type counterpart has not yet emerged owing to the challenges in the n-type doping for organic semiconductors because of its low electron affinity. On the other hand, there are ongoing efforts trying to fabricate flexible thermoelectric thin film using highly porous inorganic materials such as Bi_2Te_3. However, the thermoelectric performance was severely degraded compared with their bulk counterpart owing to the porous microstructure[8,9].

Here, we develop a strategy to synthesize n-type inorganic/organic superlattice materials with structural flexibility by organic intercalation of layered transition metal dichalcogenide TiS_2. This hybrid inorganic/organic superlattice possesses a high electronic power factor of the inorganic component TiS_2. As a result of the significant reduction in the thermal conductivity due to the organic intercalation, the in-plane ZT value has been tripled in $TiS_2[(HA)_{0.08}(H_2O)_{0.22}(DMSO)_{0.03}]$ and reached 0.28 at 373 K, which is close to that reported for the most promising p-type organic material, PEDOT–PSS. This general synthesis route using organic intercalation could be extended to many other layered two-dimensional transition metal dichalcogenides, such as MoS_2, NbS_2, TaS_2, VS_2 and CrS_2, for potentially high-ZT, both n- and p-type, flexible thermoelectric materials with abundant choice of intercalated organic compounds.

We synthesized an inorganic/organic superlattice with facile two-step chemical processes, including electrochemical intercalation and solvent exchange (Fig. 1a and Supplementary Section 1 and Supplementary Fig. 1). TiS_2 single crystals were synthesized using the chemical vapour transport method[10] and were used as the host material. The TiS_2 crystals were used as the cathode in electrochemical reaction cells with the organic salt dissolved in a solvent and used as the electrolyte. When an electrical potential was applied, part of the Ti^{4+} in TiS_2 was reduced to Ti^{3+} and the TiS_2 layers were negatively charged with additional carriers, as suggested by the X-ray photoelectron spectroscopy result (Supplementary Fig. 2). The organic cations in the electrolyte were intercalated into the van der Waals gap, driven by Coulomb force, and an inorganic/organic superlattice was formed. Owing to the cation–dipole effect, the solvent molecules are co-intercalated with the organic cations (see Supplementary Fig. 1), which can be

[1]Graduate School of Engineering, Nagoya University, Nagoya 464-8603, Japan. [2]State Key Laboratory of New Ceramics and Fine Processing, School of Materials Science and Engineering, Tsinghua University, Beijing 100084, China. [3]Department of Mechanical Engineering, University of Colorado, Boulder, Colorado 80309, USA. [4]College of Material Science and Engineering, Nanjing University of Technology, Nanjing 210009, China. [5]KOBELCO Research Institute, Kobe, Hyogo 651-2271, Japan. [6]Department of Materials Science and Engineering, Northwestern University, Evanston, Illinois 60208, USA. *e-mail: chunlei.wan@gmail.com; koumoto@apchem.nagoya-u.ac.jp

© 2015 Macmillan Publishers Limited. All rights reserved

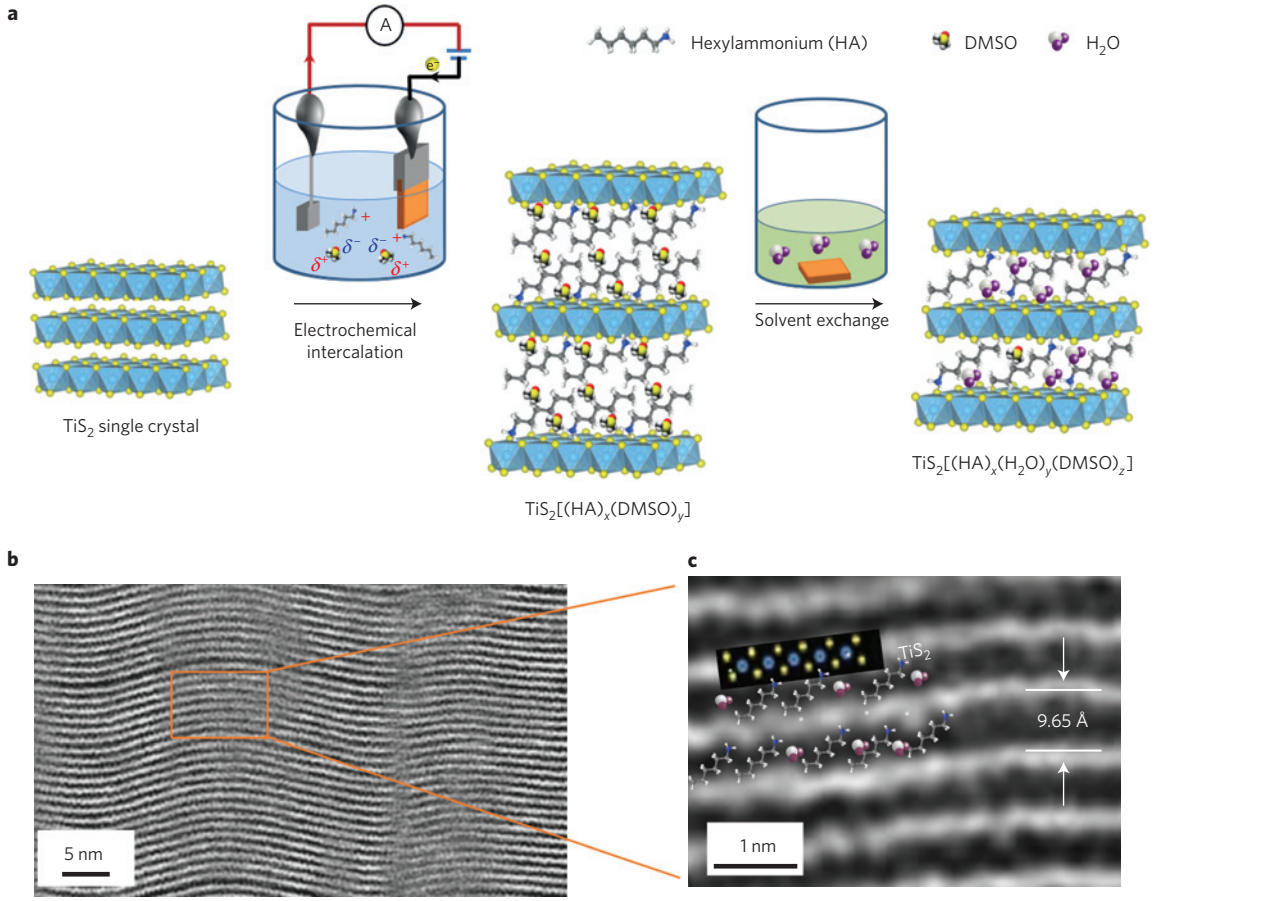

Figure 1 | Synthesis of TiS_2-based inorganic/organic superlattices. a, TiS_2 single crystal was first electrochemically intercalated into a $TiS_2[(HA)_x(DMSO)_y]$ superlattice, where a bilayer structure of the hexylammonium ions was formed owing to DMSO stabilization. A superlattice of $TiS_2[(HA)_x(H_2O)_y(DMSO)_z]$ was then formed by the solvent exchange process after immersion in water, where the hexylammonium ions change to a monolayer configuration. **b**, HAADF-STEM image of the $TiS_2[(HA)_x(H_2O)_y(DMSO)_z]$ hybrid superlattice showing a wavy structure. **c**, Magnified HAADF-STEM image of $TiS_2[(HA)_x(H_2O)_y(DMSO)_z]$.

changed into other polar solvent molecules as desired by a solvent exchange reaction[11].

Hexylammonium (HA) chloride dissolved in dimethylsulphoxide (DMSO) was chosen here as the electrolyte, which results in a hybrid superlattice of $TiS_2[(HA)_x(DMSO)_w]$ after the electrochemical intercalation reaction (Fig. 1a). The hybrid superlattice was then immersed in water to form $TiS_2[(HA)_x(H_2O)_y(DMSO)_z]$ after most of the DMSO molecules were exchanged with water molecules (Fig. 1a). Thermogravimetric differential thermal analysis was performed on the samples to study their thermal stability (Supplementary Section 2 and Supplementary Fig. 3). $TiS_2[(HA)_x(DMSO)_w]$ was found to have low thermal stability and continuously lost weight when it was heated above room temperature. In contrast, $TiS_2[(HA)_x(H_2O)_y(DMSO)_z]$ maintained its weight and was stable up to 120 °C, which is suitable for thermoelectric application around room temperature. To quantitatively determine the composition of the samples, the samples were dispersed in heavy water D_2O and mechanically crushed, then ultrasonically pulverized and heated in a sealed glass tube at 150 °C. The compositions of the hybrid superlattices were determined to be $TiS_2[(HA)_{0.19}(DMSO)_{0.35}]$ and $TiS_2[(HA)_{0.08}(H_2O)_{0.22}(DMSO)_{0.03}]$ by NMR analysis of the filtered solution containing all of the organic components (see Supplementary Section 3 and Supplementary Fig. 4). The sample microstructure was first studied by X-ray diffraction (XRD) analysis (Supplementary Fig. 5). Pure TiS_2 crystallizes with a trigonal space group ($p\bar{3}m$) and only (00l) peaks were observed perpendicular to the basal plane. The c-axis lattice constant (d), namely, the interlayer distance, was calculated to be 5.69 Å. After intercalation of the organic molecules, all of the (00l) peaks shifted to lower angles, suggesting an increase in the c-axis lattice constant and an expansion of the TiS_2 layers. The interlayer distance d became 13.97 Å for $TiS_2[(HA)_{0.19}(DMSO)_{0.35}]$, and the value decreased to 9.65 Å for $TiS_2[(HA)_{0.19}(DMSO)_{0.35}]$ after the solvent exchange. High-angle annular dark-field scanning transmission electron microscopy (HAADF-STEM) was used to observe the cross-section of the inorganic/organic superlattices. $TiS_2[(HA)_{0.19}(DMSO)_{0.35}]$ was not stable under the high vacuum environment required for transmission electron microscopy observation and thus a clear image could not be obtained. A clear image was obtained for $TiS_2[(HA)_{0.08}(H_2O)_{0.22}(DMSO)_{0.03}]$ owing to its much higher stability. In Fig. 1b,c, the bright points represent the inorganic TiS_2 layer and the dark areas represent the organic molecules, which shows that the length of the unit cell was 9.65 Å, consistent with the XRD results. The HAADF-STEM observations clearly demonstrated that the TiS_2 and organic layers stacked alternatingly, forming a stage-1 compound. As $TiS_2[(HA)_{0.08}(H_2O)_{0.22}(DMSO)_{0.03}]$ was converted from the $TiS_2[(HA)_{0.19}(DMSO)_{0.35}]$ precursor by solvent exchange reactions, it can be concluded that the latter compound is also a stage-1 compound.

HAADF-STEM can also provide information on the orientation of the hexylammonium ions with long alkyl chains. According to the shape of the dark area in Fig. 1c and the long chains in the hexylammonium molecules, the molecules were inclined by about 30° relative to the TiS_2 plane. This geometrical configuration was

© 2015 Macmillan Publishers Limited. All rights reserved

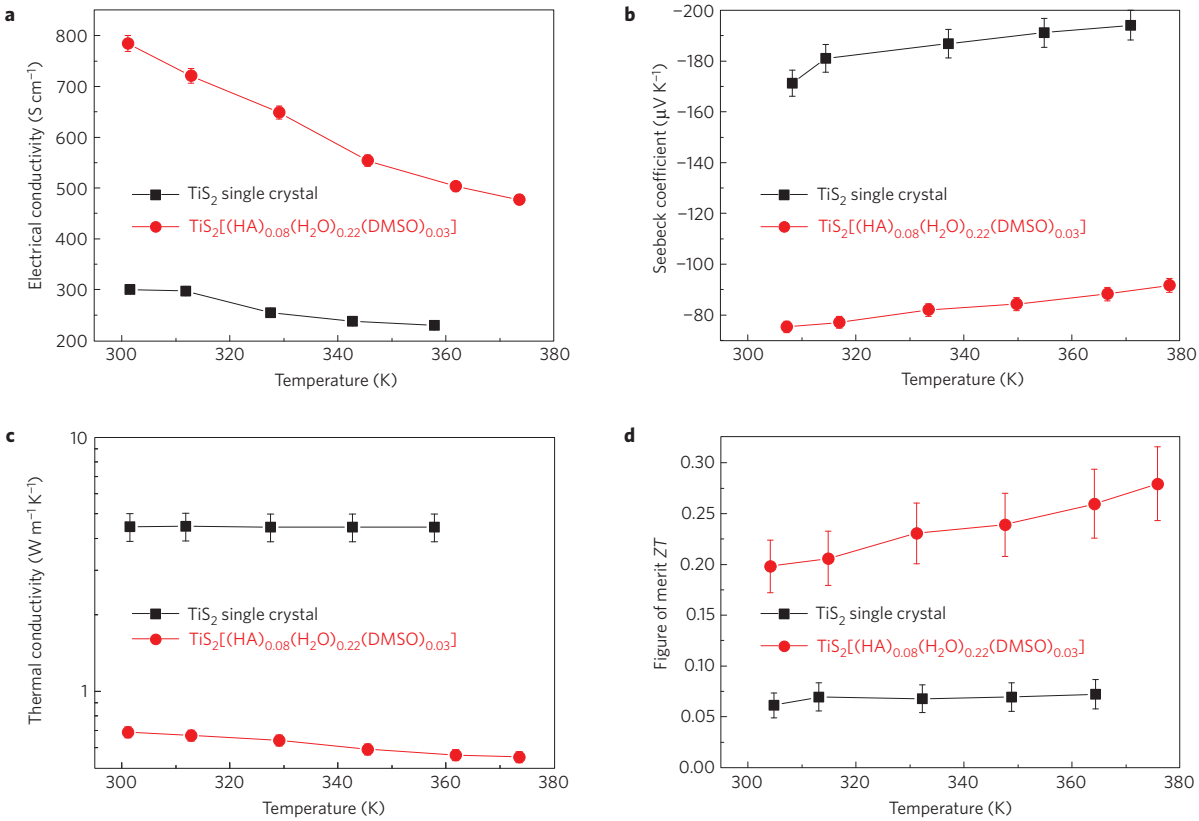

Figure 2 | Significantly enhanced in-plane thermoelectric figure of merit *ZT*. A high power factor was maintained and the thermal conductivity was decreased by about 7 times in the $TiS_2[(HA)_{0.08}(H_2O)_{0.22}(DMSO)_{0.03}]$ hybrid superlattice from the TiS_2 single crystal. **a**, In-plane electrical conductivity. **b**, In-plane Seebeck coefficient. **c**, In-plane thermal conductivity. **d**, In-plane thermoelectric figure of merit, *ZT*. Detailed error analysis is available in the Supplementary Information.

confirmed by polarized Fourier transform infrared spectroscopy (FTIR) measurements (Supplementary Section 4 and Supplementary Fig. 6). The FTIR measurement shows that the chains in the hexylammonium molecules were inclined by 31.8° relative to the TiS_2 layers in $TiS_2[(HA)_{0.08}(H_2O)_{0.22}(DMSO)_{0.03}]$, and the tilting angle of 28° was observed by polarized FTIR measurements in $TiS_2[(HA)_{0.19}(DMSO)_{0.35}]$. Considering that the expansion of the unit cell ($\Delta d = 8.28$ Å) in $TiS_2[(HA)_{0.19}(DMSO)_{0.35}]$ was almost twice that of $TiS_2[(HA)_{0.08}(H_2O)_{0.22}(DMSO)_{0.03}]$ ($\Delta d = 3.96$ Å), it can be deduced that the hexylammonium ions formed a bilayer structure in $TiS_2[(HA)_{0.19}(DMSO)_{0.35}]$ (Fig. 1a). The hydrophobic methyl groups in DMSO are compatible with the alkyl group in hexylammonium and can stabilize the paraffin-type bilayer structure[11]. However, the bilayer structure could not be maintained and a monolayer of hexylammonium ions was formed when most of the DMSO molecules were exchanged with water (Fig. 1a). Such a solvent exchange process results in a much more stable structure where the organic molecules were confined inside a narrower space between inorganic TiS_2 layers.

In Fig. 1b, the layers in the hybrid superlattice are distorted, forming a wavy structure with a nanoscale wavelength (~20 nm). It is well known that inorganic nanolayers tend to roll up and form nanotubes under a suitable treatment[12]. One driving force for the rolling up of the nanolayers is the asymmetry of their structure on the two sides of the layer[12,13]. $TiS_2[(HA)_{0.08}(H_2O)_{0.22}(DMSO)_{0.03}]$ was converted from $TiS_2[(HA)_{0.19}(DMSO)_{0.35}]$ where almost half of the hexylammonium ions were extracted during the solvent exchange reaction. The remaining hexylammonium ions may have been distributed non-uniformly on the two sides of each TiS_2 layer. The positive ammonium group at the end of the hexylammonium molecule may have aggregated, giving rise to a locally high density of positive charges. By forming a curved structure, the atomic crowding of the negatively charged sulphur atoms[14] on the inner side of the layer could compensate for this local aggregation of positive charges. As the TiS_2 monolayers in the inorganic/organic superlattice were quite large (millimetre-order), they tended to be distorted on the nanoscale instead of forming a large tube.

Figure 2 shows the in-plane thermoelectric transport properties of $TiS_2[(HA)_{0.08}(H_2O)_{0.22}(DMSO)_{0.03}]$ in comparison with those of the single crystal TiS_2 host material before organic intercalation. During the single-crystal growth, the introduction of interstitial Ti atoms readily occurred in the van der Waals gap in the TiS_2 layers and induced non-stoichiometry, resulting in additional electron carriers in the single-crystal TiS_2 (ref. 15). A carrier concentration of 3.4×10^{20} cm^{-3} was obtained by the Hall measurement for the single crystal. However, even at such high carrier concentration, the Seebeck coefficient is still very high, -171 μV K^{-1} at room temperature, owing to the high density of states of the TiS_2 conduction band that is mainly composed of three t_{2g} states of Ti 3*d* orbitals[16], where the electron carrier does not significantly alter the chemical potential. With the increasing temperature, the electrical conductivity decreased and the absolute Seebeck coefficient increased, indicating the behaviour of a typical degenerate semiconductor.

After the intercalation of the hexylammonium ions, the in-plane Seebeck coefficient decreased to -78 μV K^{-1} and the electrical conductivity increased to 790 S cm^{-1} at room temperature. During the electrochemical process, the TiS_2 layers were electrochemically reduced[17] and the negative charge was balanced by the intercalated hexylammonium ions (that is, the organic cations) according to the requirement for electrical neutrality. The total carrier density in the hybrid material increased to 7.59×10^{20} cm^{-3} after

© 2015 Macmillan Publishers Limited. All rights reserved

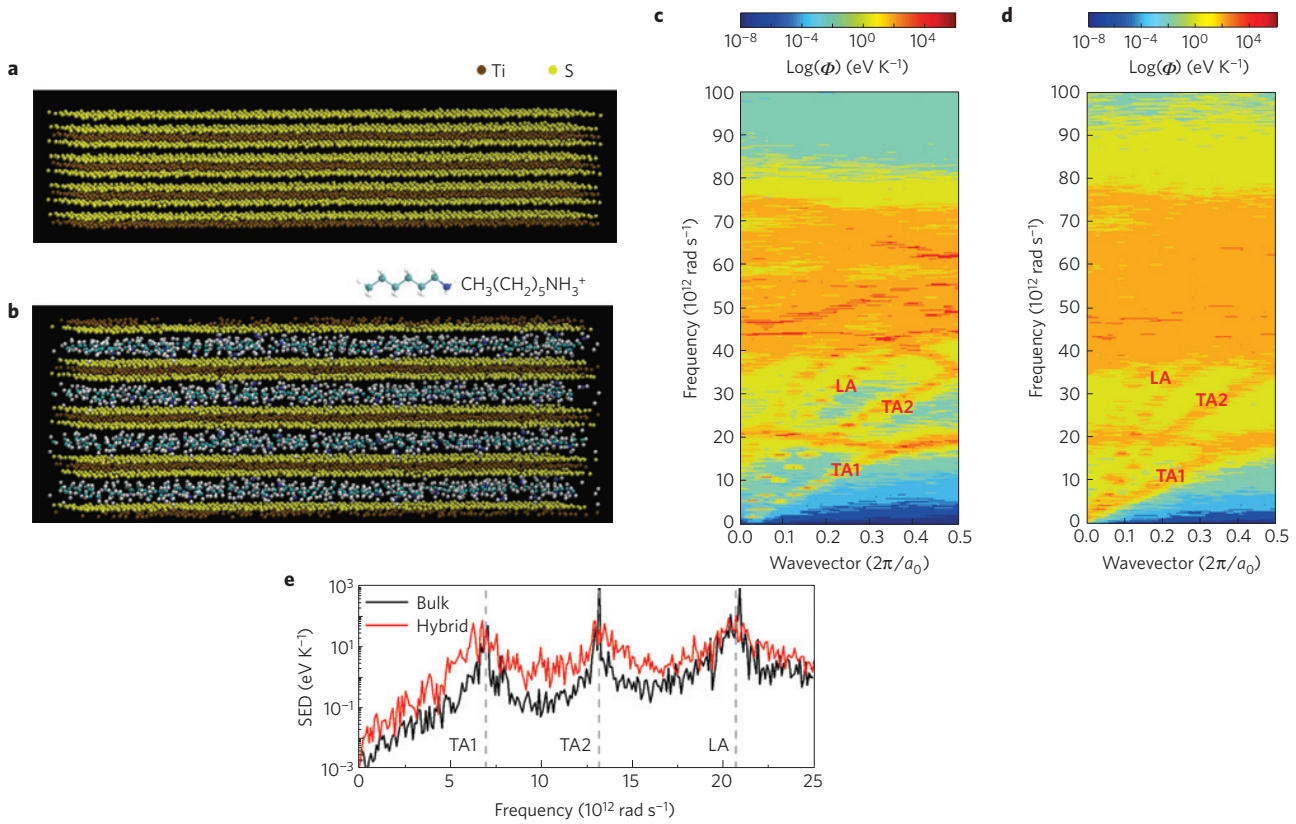

Figure 3 | Molecular dynamics simulations of the thermal conductivities. a,**b**, Structural model of TiS_2 single crystal (**a**) and the $TiS_2[(HA)_{0.08}(H_2O)_{0.22}(DMSO)_{0.03}]$ hybrid superlattice (**b**) used in molecular dynamics simulations. **c**,**d**, Spectral energy density (SED) for bulk TiS_2 single crystal (**c**) and the TiS_2 monolayer in the $TiS_2[(HA)_{0.08}(H_2O)_{0.22}(DMSO)_{0.03}]$ hybrid superlattice (**d**). Two transverse acoustic phonon branches and one longitudinal acoustic branch are labelled as TA1, TA2 and LA, respectively. **e**, SED at the wavevector ($0.25\pi/a_0$, 0, 0).

the electrochemical intercalation, as shown by the Hall measurement. This corresponds to an effective carrier concentration of 1.29×10^{21} cm^{-3} for the TiS_2 layers, if we assume that electrons are confined inside them. The in-plane mobility is calculated to be 6.41 cm^2 V^{-1} s^{-1}, using $\mu = \sigma/(nq)$, where μ, σ, n and q are mobility, electrical conductivity, carrier concentration and unit electron charge, respectively. This value is comparable to that of the TiS_2 single crystal (7.24 cm^2 V^{-1} s^{-1}), which indicates that the electron transport is still confined along the TiS_2 layers in the hybrid superlattice. The positive hexylammonium ions could potentially scatter the electrons inside the TiS_2 layers by Coulomb interaction. However, because of the presence of the polar water molecules with a high static dielectric constant ($\varepsilon_0 = 80$) that surround the positive hexylammonium ions, the Coulomb force can be effectively screened[18], and the electron mobility inside the TiS_2 layers can remain almost unaffected. Overall, the in-plane electrical transport properties of the hybrid superlattice exhibited degenerate semiconducting behaviour similar to the host single-crystal TiS_2: the electrical conductivity decreases and the absolute Seebeck coefficient increases with increasing temperature. The in-plane power factor of $TiS_2[(HA)_{0.08}(H_2O)_{0.22}(DMSO)_{0.03}]$ was 0.45 mW m^{-1} K^{-2} at room temperature, lower than that of TiS_2, 1.05 mW m^{-1} K^{-2}. However, this value is very close to the highest value reported for flexible thermoelectrics, 0.47 mW m^{-1} K^{-2} for a p-type conducting polymer PEDOT–PSS (ref. 7), and much higher than that of n-type organometallic poly(K_x(Ni-1,1,2,2-ethenetetrathiolate)) (0.07 mW m^{-1} K^{-2}; ref. 19) and n-type (Zn,Al)O/hydroquinone hybrid material[20] (0.018 mW m^{-1} K^{-2}). It is even higher than that of a flexible inorganic Bi_2Te_3 thin film[8] (0.18 mW m^{-1} K^{-2}) where the porous structure was introduced to increase the flexibility, which also severely deteriorates the electrical conductivity.

The in-plane thermal conductivities of the TiS_2 single crystal and $TiS_2[(HA)_{0.08}(H_2O)_{0.22}(DMSO)_{0.03}]$ were measured to be 4.45 W m^{-1} K^{-1} and 0.69 W m^{-1} K^{-1} using the parallel thermal conductance method developed for small samples[21], respectively (see Supplementary Section 5 and Supplementary Fig. 7 for details). The experimental value of the TiS_2 single crystal is close to the literature value[22]. As a result of the significant reduction in the thermal conductivity, the in-plane ZT value has been tripled in $TiS_2[(HA)_{0.08}(H_2O)_{0.22}(DMSO)_{0.03}$ and reached 0.28 at 373 K, which is the highest for n-type flexible thermoelectrics and is close to that of the most promising p-type organic material, PEDOT–PSS (ref. 7).

Both phonons and electrons contribute to the thermal conductivity, and the electronic contribution can be comparable to the phonon contribution in high-efficiency thermoelectric materials. After subtracting the electronic thermal conductivity that was estimated according to the Wiedemann–Franz law using a calibrated Lorentz constant (see Supplementary Section 8), the in-plane lattice thermal conductivity was estimated to be 4.2 W m^{-1} K^{-1} for the TiS_2 single crystal and an ultralow value of 0.12 W m^{-1} K^{-1} was obtained for $TiS_2[(HA)_{0.08}(H_2O)_{0.22}(DMSO)_{0.03}]$ at 300 K. The ultralow thermal conductivities across inorganic/organic interfaces have been studied for planar self-assembled monolayers[23] and nanocrystal arrays[24]. Low cross-plane thermal conductivity has also been reported for inorganic/organic superlattices[25,26]. However, the in-plane thermal conductivity of inorganic/organic superlattices has not been reported. Assuming the TiS_2 layers and the organic molecules formed a parallel thermal circuit along the in-plane direction of the hybrid superlattice, the thermal conductivity was estimated to be 2.59 W m^{-1} K^{-1}, almost half of the thermal conductivity of bulk TiS_2, which is much higher than the measured value.

© 2015 Macmillan Publishers Limited. All rights reserved

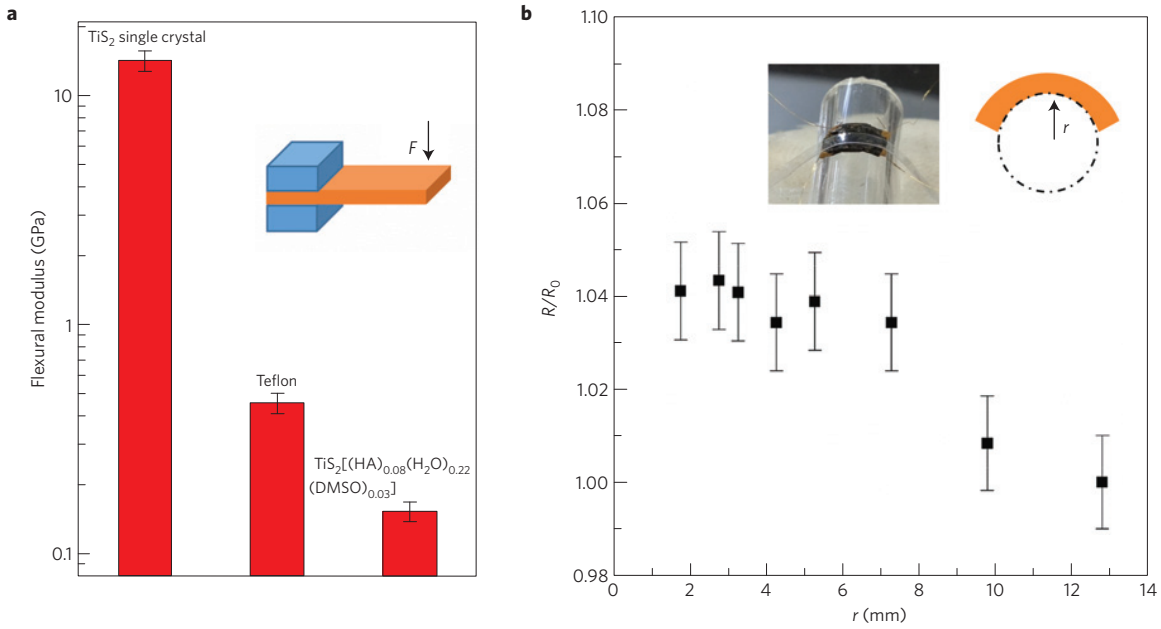

Figure 4 | Flexibility tests. a, The flexural modulus of the $TiS_2[(HA)_{0.08}(H_2O)_{0.22}(DMSO)_{0.03}]$ hybrid superlattice is two orders of magnitude lower than that of TiS_2 and is even lower than that of a typical plastic material, Teflon. *F* represents the applied force for bending the sample in the measurement. **b**, The sheet resistance *R* as a function of bending radius (*r*) for a 0.3-mm-thick $TiS_2[(HA)_{0.08}(H_2O)_{0.22}(DMSO)_{0.03}]$ crystal, where R_0 is the corresponding value of its original state before bending. Detailed error analysis is available in the Supplementary Information.

To explain such ultralow thermal conductivity of $TiS_2[(HA)_{0.08}(H_2O)_{0.22}(DMSO)_{0.03}]$, we conduct the equilibrium molecular dynamics simulations with the Green–Kubo method to understand the fundamental phonon transport mechanisms in both bulk TiS_2 and the hybrid superlattice material with hexylammonium molecules. The details of interatomic potential parameters and computation methodology can be found in Supplementary Section 9 and Supplementary Fig. 10, and the Supplementary Movie. In our simulations, we observed an eightfold reduction in lattice thermal conductivity when the TiS_2 bulk is intercalated by organic components. This reduction is significantly higher than the simple volumetric averaging, indicating that the coupling between the inorganic and organic parts plays an important role in phonon transport in the in-plane direction. As the thermal conduction in the inorganic part is much better than the organic part, the low thermal conductivity of the hybrid material could be attributed to the reduction in the thermal conductivity of the inorganic layer after the intercalation. To qualitatively explain the difference in the phonon dynamics between bulk TiS_2 and the hybrid material, we calculate the spectral energy density[27], $\phi(\mathbf{k},\omega)$ with phonon wavevector $\mathbf{k}$ and frequency ω of the bulk TiS_2 and the TiS_2 layer from the hybrid material, as shown in Fig. 3a–d. The positions of peaks, ω_0, in the spectral energy density distribution for a given wavevector, $\mathbf{k}_0$, correspond to the phonon dispersion that the material supports, and the broadening of the peak in the frequency domain is related to the phonon relaxation time. The smaller the broadening is, the longer is the relaxation time. In both materials, the three acoustic branches are clearly distinguishable. For all acoustic dispersions, larger broadening can be observed for the hybrid case. Figure 3e shows the spectral energy density at $(0.25\pi/a_0, 0, 0)$ as an example, indicating the increased phonon scattering rates in the hybrid material. The stronger scattering in the hybrid material can be understood as a result of the inorganic TiS_2 layers being ionically combined with the dangling hexylammonium ions. The electrostatic interaction is much stronger than weak van der Waals interaction, which is dominant in the bulk TiS_2.

It is noted that the degree of reduction in the thermal conductivity obtained in the present equilibrium molecular dynamics simulations is still less than the experimental observation. This is because other scattering mechanisms besides the interfacial coupling can potentially further reduce the thermal conductivity, which is worthy of further investigation. One possibility is the wavy structure of the layers observed in Fig. 1. As a reference, we measured the thermal conductivity of $TiS_2[(HA)_x(PEG)_y]$, where the layers were aligned straight owing to the long chain structure of polyethylene glycol (PEG; see Supplementary Section 10 and Supplementary Fig. 11). The lattice thermal conductivity of the flat hybrid superlattice $TiS_2[(HA)_x(PEG)_y]$ was measured to be 0.56 $W\,m^{-1}\,K^{-1}$, 4–5 times higher than the wavy $TiS_2[(HA)_{0.08}(H_2O)_{0.22}(DMSO)_{0.03}]$. This can be further explained using the thermal conductivity accumulation as a function of mean free path (see Supplementary Fig. 10e). The phonons with a mean free path above 10 nm (the half-wavelength of the wavy structure) that contribute to 82% of the total thermal conductivity would be strongly scattered by the wavy structure. In addition, local atomic disordering of the TiS_2 layers in the hybrid superlattice in the wavy structure could be another additional phonon scattering mechanism. Compared with the sharp peaks of XRD for TiS_2 single crystals, the peaks of $TiS_2[(HA)_{0.08}(H_2O)_{0.22}(DMSO)_{0.03}]$ become broadened (Supplementary Fig. 5), which is a sign of structural disordering as further confirmed by HAADF-STEM (Supplementary Fig. 12).

Apart from the low thermal conductivity, the hybrid superlattice became mechanically flexible compared with a TiS_2 single crystal. The flexural modulus was measured to be ~145 MPa at 300 K, which is two orders of magnitude lower than that of a TiS_2 single crystal and even lower than a typical plastic material (such as Teflon), as shown in Fig. 4a. In the TiS_2 single crystal, the TiS_2 layers were connected by van der Waals forces, but the interlayer interaction was significantly reduced by the expansion of the interlayers, as a result of the intercalation of organic molecules. Moreover, the organic molecules that occupy the space between neighbouring TiS_2 layers could also accommodate deformations and contribute to the flexibility. Therefore, the two-dimensional TiS_2 monolayers could be freely deformed and were highly flexible. When the material was attached to the surfaces of glass tubes with different radii, the electrical resistance slightly changed under bending deformation,

© 2015 Macmillan Publishers Limited. All rights reserved

within 5% of the resistance of the original state, even when the bending radius was 1.5 mm (Fig. 4b). This result firmly suggests that the material can be attached to any curved surface to fabricate flexible thermoelectric generators or coolers.

In summary, we present a new approach to synthesize n-type flexible thermoelectric materials through a facile electrochemical intercalation method to fabricate a hybrid superlattice of alternating inorganic TiS_2 monolayers and organic cations. This general synthesis route using organic intercalation could become a platform to fabricate hybrid inorganic/organic superlattices that would lead to the discovery of new, flexible, high-efficiency thermoelectric materials. Many other layered materials such as Bi_2Te_3 or the transition metal dichalcogenides NbS_2, TaS_2, VS_2, CrS_2, MoS_2, or even layered oxides such as Na_xCoO_2 could also be intercalated to make both n- and p-type thermoelectric materials. The infinite choices of organic molecules with various sizes and functional groups could further diversify the compositions and provide strategies to optimize the thermoelectric performance, such as dimension control[28] and dielectric engineering[18].

Methods

TiS_2 single crystals with a typical size of 4 mm × 4 mm × 100 μm were grown by the chemical vapour transport method using excess sulphur as the transport agent[10]. The hybrid inorganic/organic superlattices were then synthesized using an electrochemical intercalation process and subsequent solvent exchange processes (see Supplementary Section 1 and Supplementary Fig. 1). The obtained samples were vacuum dried for 24 h and then characterized by XRD, thermogravimetric differential thermal analysis and X-ray photoemission spectroscopy. To quantitatively determine the composition of the samples, the samples were dispersed in heavy water D_2O and mechanically crushed, then ultrasonically pulverized and heated in a sealed glass tube at 150 °C. The compositions of the hybrid superlattices were determined by NMR analysis of the filtered solution containing all of the organic components. The hybrid material was ultrasonically pulverized and a thin film was prepared by dropping the dispersion solution onto the surface of a CaF substrate and analysed by FTIR to determine the orientation of the hexylammonium molecules. The cross-sections of the samples were observed by HAADF-STEM. All of the transport properties were measured on the same sample, in the sequence of thermal conductivity, Seebeck coefficient, electrical conductivity and Hall measurements (TOYO Corporation, ResiTest8300). The details of the measurement of thermal conductivity, Seebeck coefficient and electrical conductivity are discussed in Supplementary Sections 5–7 and Supplementary Figs 7–9. The bending modulus was also measured by a home-made apparatus introduced in Supplementary Section 11 and Supplementary Fig. 13. Flexibility was evaluated by attaching the hybrid superlattice to the surfaces of glass tubes with different radii and measuring the resistivity using the van der Pauw method. Classical molecular dynamics simulations are performed using the LAMMPS package for the phononic thermal conductivity (see Supplementary Section 9).

Received 24 July 2014; accepted 19 February 2015; published online 6 April 2015

References

1. Dimitrakopoulos, C. D. & Malenfant, P. R. L. Organic thin film transistors for large area electronics. *Adv. Mater.* **14,** 99–117 (2002).
2. Janata, J. & Josowicz, M. Conducting polymers in electronic chemical sensors. *Nature Mater.* **2,** 19–24 (2003).
3. Ouyang, J. Y., Chu, C. W., Szmanda, C. R., Ma, L. P. & Yang, Y. Programmable polymer thin film and non-volatile memory device. *Nature Mater.* **3,** 918–922 (2004).
4. Burroughes, J. H. *et al.* Light-emitting-diodes based on conjugated polymers. *Nature* **347,** 539–541 (1990).
5. Sariciftci, N. S., Smilowitz, L., Heeger, A. J. & Wudl, F. Photoinduced electron-transfer from conducting polymer to buckminsterfullerene. *Science* **258,** 1474–1476 (1992).
6. Bubnova, O. *et al.* Optimization of the thermoelectric figure of merit in the conducting polymer poly(3,4-ethylenedioxythiophene). *Nature Mater.* **10,** 429–433 (2011).
7. Kim, G. H., Shao, L., Zhang, K. & Pipe, K. P. Engineered doping of organic semiconductors for enhanced thermoelectric efficiency. *Nature Mater.* **12,** 719–723 (2013).
8. Lu, Z. Y. *et al.* Fabrication of flexible thermoelectric thin film devices by inkjet printing. *Small* **10,** 3551–3554 (2014).
9. Yadav, A., Pipe, K. P. & Shtein, M. Fiber-based flexible thermoelectric power generator. *J. Power Sources* **175,** 909–913 (2008).
10. Barry, J. J., Hughes, H. P., Klipstein, P. C. & Friend, R. H. Stoichiometry effects in angle-resolved photoemission and transport studies of $Ti_{1+x}S_2$. *J. Phys.* **16,** 393–402 (1983).
11. Schollho, R. & Weiss, A. Cation-exchange reactions and layer solvate complexes of ternary phases M_xMoS_2. *J. Less-Common Met.* **36,** 229–236 (1974).
12. Li, Y. D. D., Li, X. L. L., He, R. R. R., Zhu, J. & Deng, Z. X. X. Artificial lamellar mesostructures to WS_2 nanotubes. *J. Am. Chem. Soc.* **124,** 1411–1416 (2002).
13. Ferrari, A. M., Szieberth, D., Zicovich-Wilson, C. M. & Demichelis, R. Anatase(001) 3 ML nanotubes, the first TiO_2 nanotube with negative strain energies: A DFT prediction. *J. Phys. Chem. Lett.* **1,** 2854–2857 (2010).
14. Tibbetts, K., Doe, R. & Ceder, G. Polygonal model for layered inorganic nanotubes. *Phys. Rev. B* **80,** 014102 (2009).
15. Kukkonen, C. A. *et al.* Transport and optical-properties of $Ti_{1+x}S_2$. *Phys. Rev. B* **24,** 1691–1709 (1981).
16. Fang, C. M., deGroot, R. A. & Haas, C. Bulk and surface electronic structure of 1T-TiS_2 and 1T-$TiSe_2$. *Phys. Rev. B* **56,** 4455–4463 (1997).
17. Schollho, R. & Meyer, H. Cathodic reduction of layered transition-metal chalcogenides. *Mater. Res. Bull.* **9,** 1237–1246 (1974).
18. Jena, D. & Konar, A. Enhancement of carrier mobility in semiconductor nanostructures by dielectric engineering. *Phys. Rev. Lett.* **98,** 136805 (2007).
19. Sun, Y. M. *et al.* Organic thermoelectric materials and devices based on p- and n-type poly(metal 1,1,2,2-ethenetetrathiolate)s. *Adv. Mater.* **24,** 932–937 (2012).
20. Tynell, T., Terasaki, I., Yamauchi, H. & Karppinen, M. Thermoelectric characteristics of (Zn,Al)O/hydroquinone superlattices. *J. Mater. Chem. A* **1,** 13619–13624 (2013).
21. Zawilski, B. M., Littleton, R. T. & Tritt, T. M. Description of the parallel thermal conductance technique for the measurement of the thermal conductivity of small diameter samples. *Rev. Sci. Instrum.* **72,** 1770–1774 (2001).
22. Imai, H., Shimakawa, Y. & Kubo, Y. Large thermoelectric power factor in TiS_2 crystal with nearly stoichiometric composition. *Phys. Rev. B* **64,** 241104 (2001).
23. Losego, M. D., Grady, M. E., Sottos, N. R., Cahill, D. G. & Braun, P. V. Effects of chemical bonding on heat transport across interfaces. *Nature Mater.* **11,** 502–506 (2012).
24. Ong, W. L., Rupich, S. M., Talapin, D. V., McGaughey, A. J. H. & Malen, J. A. Surface chemistry mediates thermal transport in three-dimensional nanocrystal arrays. *Nature Mater.* **12,** 410–415 (2013).
25. Losego, M. D., Blitz, I. P., Vaia, R. A., Cahill, D. G. & Braunt, P. V. Ultralow thermal conductivity in organoclay nanolaminates synthesized via simple self-assembly. *Nano Lett.* **13,** 2215–2219 (2013).
26. Liu, J. *et al.* Ultralow thermal conductivity of atomic/molecular layer-deposited hybrid inorganic/organic zincone thin films. *Nano Lett.* **13,** 5594–5599 (2013).
27. Thomas, J. A., Turney, J. E., Iutzi, R. M., Amon, C. H. & McGaughey, A. J. Predicting phonon dispersion relations and lifetimes from the spectral energy density. *Phys. Rev. B* **81,** 081411 (2010).
28. Harshman, D. R. & Mills, A. P. Concerning the nature of high-T_C superconductivity—survey of experimental properties and implications for interlayer coupling. *Phys. Rev. B* **45,** 10684–10712 (1992).

Acknowledgements

The authors thank R. Sasai for polarized FTIR measurements. C.W. acknowledges financial support from a Murata Science Foundation Research Grant, a Thermal and Electrical Energy Technology Foundation Research Grant, Takahashi Industrial and Economic Research Foundation and JSPS KAKENHI Grant Number 26820295. K.Koumoto acknowledges financial support from JSPS KAKENHI Grant Number 25289226 and TherMAT. G.J.S. acknowledges support from AFOSR-MURI and DOE-EFRC (S3TEC) award number DE-SC0001299. X.G. and R.Y. acknowledge the partial support for this work from the NSF CAREER award (0846561) and AFOSR (FA9550-11-1-0109). The simulation work used the Janus supercomputer, supported by NSF (0821794).

Author contributions

C.W. and K.Koumoto initiated the concepts. C.W. designed the experiments. C.W., F.D., T.I., Y.W., H.S., M.K., K.Koga and K.Y. conducted the experiments. X.G. and R.Y. performed the molecular dynamics simulations. C.W., X.G., G.J.S., R.Y. and K.Koumoto analysed the data and wrote the manuscript. All of the authors contributed to manuscript preparation.

Additional information

Supplementary information is available in the online version of the paper. Reprints and permissions information is available online at www.nature.com/reprints. Correspondence and requests for materials should be addressed to C.W. or K.K.

Competing financial interests

The authors declare no competing financial interests.

© 2015 Macmillan Publishers Limited. All rights reserved